Nanostructural Evolution under Reducing Conditions of a Pt/CeTbO$_x$ Catalyst: A New Alternative System as a TWC Component

G. Blanco, J. J. Calvino,* M. A. Cauqui, P. Corchado, and C. López-Cartes

Departamento de Ciencia de los Materiales e Ingeniería Metalúrgica y Química Inorgánica, Facultad de Ciencias, Universidad de Cádiz, Polígono Rio San Pedro s/n, Apdo 40 Puerto Real, Cádiz-11510, Spain

C. Colliex,† J. A. Pérez-Omil, and O. Stephan

Laboratoire de Physique des Solides, CNRS URA 002, Université Paris-Sud, Batiment 510, 91405 Orsay Cedex, France

Received July 5, 1999. Revised Manuscript Received September 30, 1999

By using a combination of high resolution electron microscopy (HREM) and nanoanalytical electron microscopy (EELS-STEM) techniques, the nanoscale evolution of a 5% Pt/$Ce_{0.8}Tb_{0.2}O_{2-x}$ catalyst submitted to reduction in pure hydrogen within the 423−1173 K range has been investigated. Fine details about the platinum catalytic particles, such as their bulk and surface chemical state, size, shape, or structural relationships with the mixed-oxide support, have been established and their change with reduction temperature monitored. Results indicate that at low reduction temperatures (<773 K) platinum is present in this catalyst in the form of well-faceted metallic particles with clean surfaces. At higher reduction temperatures drastic transformations have been detected. Thus after 1-h reduction at 973 K the decoration of the metal particle surfaces by the support takes place, while after reduction at 1173 K the formation of an intermetallic compound, with $LnPt_5$ (Ln = Ce, Tb) stoichiometry, occurs. The interpretation of HREM images by image simulation has allowed us to determine the morphology of the intermetallic crystals as being of the beryl-type. Specific orientation relationships between the mixed-oxide support and the intermetallic have also been established by comparing experimental and simulated HREM images, as well as from the analysis of selected area diffraction patterns. Electron energy loss spectra confirm that in the mixed-oxide used as support, cerium and terbium are homogeneously distributed. No phase segregation was observed either in the nonreduced catalysts or in the catalysts resulting from reduction treatments in the whole range of T_{red} here studied. In the sample reduced at 1173 K, the analysis of the fine structure of EELS spectra recorded across the interface between the support and the supported particles confirms the formation of an intermetallic phase and reveals a preferential incorporation of Ce in these particles. The oxidation state of Ce in the intermetallic is markedly lower than that observed in the support.

1. Introduction

Noble metal/CeO_2 systems have been widely studied because of their value as a three-way catalyst (TWC) component. It is generally acknowledged that chemisorption techniques cannot be applied in a conventional way for the straightforward characterization of these systems. First, the support itself can strongly adsorb the most usual probe molecules such as H_2 or CO. Second, the reducibility of ceria make these catalysts prone to show metal−support interaction effects.[1−3] Both arguments advocate the use of instrumental techniques to obtain a more direct insight into the nanostructural catalyst features.[4−6]

High resolution electron microscopy (HREM) is a powerful tool for investigating the nanostructural features of highly dispersed metal catalysts. Information concerning metal particle size and morphology, metal−support structural relationships, metal decoration (partial covering of the metal crystallites by support), and

* Corresponding author: Telephone: + 34 956 01 63 33. Fax: + 34 956 01 6822. E-mail: jose.calvino@uca.es.

† Also at Laboratoire Aimé Cotton, CNRS UPR 3321, Université Paris-Sud, Batiment 505, 91405 Cedex, France.

(1) Meriaudeau, P.; Dutel, J. F.; Dufaux, M.; Naccache, C. *Strong metal support interactions*; ACS Symp. Serv. 298; American Chemical Society: Washington DC, 1986; p 118.

(2) Barrault, J.; Alouche, A.; Paul-Boncour, V.; Hilaire, L.; Percheron-Guegan, A. *Appl. Catal.* **1989**, *46*, 269.

(3) Pfau, A.; Sanz, J.; Schierbaum, K. D.; Göpel, W.; Belzunegui, J. P.; Rojo, J. M. *Stud. Surf. Sci. Catal.* **1996**, *101*, 931.

(4) Bernal, S.; Botana, F. J.; García, R.; Kang, Z. C.; López, M. L.; Pan, M.; Ramírez, F.; Rodríguez-Izquierdo, J. M. *Catal. Today* **1988**, *2*, 653.

(5) Bernal, S.; Calvino, J. J.; Cifredo, G. A.; Rodríguez-Izquierdo, J. M.; Perrichon, V.; Laarchir, A. *J. Catal.* **1992**, *137*, 1.

(6) Sanz, J.; Belzunegui, J. P.; Rojo, J. M. *J. Am. Chem. Soc.* **1992**, *114*, 6749.

10.1021/cm991093q CCC: $18.00
Published on Web 12/01/1999

alloying effects can be obtained. In previous papers, we have shown that HREM can be helpful in characterizing in depth the metal dispersion and other features relevant to structural aspects of the noble metal/ceria interaction.[4,5,7−13] From these studies, a better understanding of the deactivation mechanisms operating in these NM/CeO_2 systems (sintering, decoration effects, alloying processes) and to some extent in TWCs has been gained.

In this paper, the background developed in our lab for HREM image interpretation[14,15] is applied to the study of metal−support interaction effects on a Pt/CeTbO$_x$ catalyst showing promising advantages as a TWC component compared to Pt/CeO_2. Thus, in recent reports,[16,17] we have shown that CeTbO$_x$ exhibits better oxygen buffering capacity (OBC) than NM/CeO_2 and that the temperature range in which the mixed oxide is active as a buffer is broader and shifted to lower temperatures. Other authors have also observed improvements in properties for other TWC model systems constituted by noble metals dispersed on ceria-based mixed oxides containing other trivalent cations,[18−21] but in our view those noted for CeTbO$_x$ are particularly significant.[22]

As the reduction of the CeTbO$_x$ mixed oxide starts at a significantly lower temperature than that of CeO_2,[22] and as the same trend remains when NM are supported on them,[23] we considered it interesting to trace the structural changes in Pt/CeTbO$_x$ for increasing reduction temperatures, following treatments similar to those previously used for NM/CeO_2.

More specifically, herein we report on the nanostructural evolution of a 5% Pt/CeTbO$_x$ catalyst subjected to reduction at temperatures in the range 423−1173 K. By using a combination of high-resolution electron microscopy and computational image calculation techniques, the critical nanostructure/thermochemical treatment relationships for the system investigated here have been elucidated. The sequence of changes taking place on the catalyst as a function of the reduction treatment should be considered in the future for the rational design of the new generation of TWC materials.

The results shown here provide a very good insight into the power of combining digital image processing and image simulation techniques for interpreting very fine structural details in these complex systems. This task, which is crucial for a further understanding of the chemistry of these catalysts, can be accomplished using the software tools developed in our lab to build up models in which features such as the size, shape, chemical nature, and orientation of the dispersed particles, as well as the nature, thickness, and structural defects characterizing the support can be very flexibly included. Such models are the inputs for the simulation programs which allow reproduction of the distinctive features observed in the experimental images.

The structural information obtained from HREM is complemented by a parallel nanoanalytical study by electron energy loss spectroscopy (EELS), carried out in a dedicated scanning transmission microscope (STEM) equipped with a field emission tip as electron source. The subnanometric, high-energy, electron probe that is generated in such microscopes constitutes a unique tool for investigating the chemical and structural features of specimens at a very fine spatial scale.[24−26] This probe can be either positioned or scanned along a precise path through the sample, providing in this way information about changes of composition and of structural-electronic properties of the catalyst, which cannot be determined using conventional TEM or HREM techniques. In this particular contribution, this technique has been used to unveil the compositional features of the catalyst reduced at the highest temperature employed in this study, 1173 K.

2. Experimental Section

The Ce−Tb mixed oxide employed as a support for platinum in the present work was prepared by coprecipitation from an aqueous solution of the corresponding nitrates, after addition of concentrated ammonium hydroxide. For this purpose, stoichiometric amounts of $Tb(NO_3)_3 \cdot 5H_2O$ and $Ce(NO_3)_3 \cdot 6H_2O$, both 99.99% pure from Aldrich, were dissolved separately in distilled water, and the resulting solutions were mixed. A 25% ammonia solution, from Merck, slowly added to the nitrate mixture was used as precipitating agent. The solid thus obtained was washed, filtered, and oven-dried for 12 h at 403 K. After the dried product was milled and ground, a final calcination step was applied to decompose the mixed-oxide precursor. Specifically, a treatment in air for 2 h at high temperature, 1173 K, was selected in order to get a Ce−Tb mixed oxide with stable surface area. By doing this, metal particle encapsulation processes, during further reduction treatments in hydrogen at high temperature, can be minimized.

By using the procedure described above, a homogeneous $Ce_{0.8}Tb_{0.2}O_{2-x}$ mixed oxide, hereafter referred to as CeTbO$_x$, with 8 $m^2\ g^{-1}$ BET surface area was prepared. The chemical composition of this oxide was also checked by ICP.[20] XRD

(7) Bernal, S.; Botana, F. J.; Calvino, J. J.; Cifredo, G. A.; Pérez-Omil, J. A.; Pintado, J. M. *Catal. Today* **1995**, *23*, 219.
(8) Bernal, S.; Calvino, J. J.; Cauqui, M. A.; Gatica, J. M.; Larese, C.; Pérez-Omil, J. A.; Pintado, J. M. *Catal. Today* **1999**, *50*, 175.
(9) Bernal, S.; Calvino, J. J.; Gatica, J. M.; Larese, C.; López-Cartes, C.; Pérez-Omil, J. A. *J. Catal.* **1997**, *169*, 510.
(10) Bernal, S.; Blanco, G.; Calvino, J. J.; Cifredo, G. A.; Pérez-Omil, J. A.; Pintado, J. M.; Varo, A. *Stud. Surf. Sci. Catal.* **1994**, *82*, 507.
(11) Bernal, S.; Calvino, J. J.; Cauqui, M. A.; Pérez-Omil, J. A.; Pintado, J. M.; Rodríguez-Izquierdo, J. M. *Appl. Catal. B* **1998**, *16*, 127.
(12) Bernal, S.; Calvino, J. J.; Cauqui, M. A.; Cifredo, G. A.; Jobacho, A.; Rodríguez-Izquierdo, J. M. *Appl. Catal.* **1993**, *99*, 1.
(13) Bernal, S.; Cauqui, M. A.; Cifredo, G. A.; Gatica, J. M.; Larese, C.; Pérez-Omil, J. A. *Catal. Today* **1996**, *29*, 77.
(14) Bernal, S.; Botana, F. J.; Calvino, J. J.; López-Cartes, C.; Pérez-Omil, J. A.; Rodríguez-Izquierdo, J. M. *Ultramicroscopy* **1998**, *72*, 135.
(15) Botana, F. J.; Calvino, J. J.; Blanco, G.; Marcos, M. *Proc. ICEM 13 Paris (France), Electron Microscopy* **1994**, *Vol. 2B*, 1077.
(16) Bernal, S.; Blanco, G.; Cauqui, M. A.; Corchado, P.; Pintado, J. M.; Rodríguez-Izquierdo, J. M. *Chem. Commun.* **1997**, 1545.
(17) Bernal, S.; Blanco, G.; Cauqui, M. A.; Corchado, P.; Pintado, J. M.; Rodríguez-Izquierdo, J. M.; Vidal, H. *Stud. Surf. Sci. Catal.* **1998**, *116*, 611.
(18) Logan, A. D.; Shelef, M. *J. Mater. Res.* **1994**, *9* (2), 468.
(19) Miki, T.; Ogawa, T.; Haneda, M.; Kakuta, N.; Ueno, A.; Tateishi, S.; Matsuura, S.; Sato, M. *J. Phys. Chem.* **1990**, *94*, 6464.
(20) Cho, B. K. *J. Catal.* **1991**, *131*, 74.
(21) Japan Kokai Tokkyo Koho JP Nos., 63-240947, 63-104651, 63-84636, 63-77545, 62-282640, 61-293550, and 61-197038.
(22) Blanco, G. Ph.D. dissertation, Universidad de Cádiz, 1997.
(23) Bernal, S.; Blanco, G.; Cauqui, M. A.; Corchado, P.; Larese, C.; Pintado, J. M.; Vidal, H. *Catal. Today*, in press.
(24) Suenaga, K.; Colliex, C.; Demoncy, N.; Loiseau, A.; Pascard, H.; Willaime, F. *Science* **1997**, *278*, 653.
(25) Tence, M.; Quartuccio, M.; Colliex, C. *Ultramicroscopy* **1995**, *58*, 42.
(26) Mory, C.; Stephan, O.; Tencé, M.; Colliex, C. *Proc. ICEM 14 Cancún (México), Electron Microscopy* **1998**, *Vol. II*, 455. IoP Bristol and Philadelphia.

diagrams corresponding to the calcined sample showed the peaks characteristic of a cubic, fluorite-type structure with a lattice constant about 0.5404 nm.[20] Further characterization details about this oxide can be found in refs 16 and 17.

Starting from this mixed oxide, the 5% Pt/$CeTbO_x$ catalyst was prepared by incipient impregnation with an aqueous solution of $[Pt(NH_3)_4](OH)_2$. After impregnation, the catalyst was dried in oven at 383 K for 12 h and stored in a desiccator.

The reduction treatments applied to the catalyst precursor were done in pure flowing hydrogen (60 cm^3 min^{-1}) at a heating rate of 5 K min^{-1}. The catalyst was held for 1 h at the selected reduction temperature (423, 773, 973, or 1173 K) and further evacuated at the reduction temperature for 1 h in a flow of helium. The microscopy samples were prepared and transferred into the microscope as described in ref 7.

Experimental HREM images were recorded in a JEOL-2000EX electron microscope, operating at 200 kV, with a structural resolution of 0.21 nm. Simulated images were calculated using the EMS software[27] and the structural models built with the RHODIUS program developed at the University of Cadiz,[15] both running on a INDY 4400SC Silicon Graphics Workstation. Image processing, mainly FFT analysis of the micrographs, was accomplished using the SEMPER 6+ package by Synoptics Ltd., on images digitized with a COHU-4910 CCD camera. The diffractograms or digital diffraction patterns (DDPs) included in this work correspond to the power spectrum of the Fourier transform of the bidimensional intensity distribution in the digitized images.

The nanoanalytical information was obtained in a VG-HB501 scanning transmission microscope (STEM) operating at 100 kV, equipped with a field emision gun and a parallel detection electron energy loss spectrometer (Gatan PEELS 666). EELS spectra were processed with the EL/P program from Gatan. Specific routines developed at the Laboratoire de Physique de Solides at Orsay (Paris) were also used for on-line electron beam control during the acquisition of experimental line-scan spectra.

3. Results and Discussion

3.1. The Structure of 5% Pt/$CeTbO_x$ Catalyst after Reduction at Low Temperatures (423−773 K). Figures 1 and 2 show experimental HREM views depicting the main nanostructural features of the 5% Pt/$CeTbO_x$ catalyst after reduction treatments at low temperatures, 423 and 773 K, respectively. In all the images contained in these figures, small particles deposited on the surface of larger, mixed-oxide support, crystals are clearly visible.

To identify the chemical nature of the nanometer-sized particles observed in the catalyst reduced at 423 K, an analysis of their lattice fringes was performed on the basis of digital diffraction patterns (DDPs). Using this procedure, the cross fringes observed in the particles of Figure 1a were assigned to the [110] zone axis of metallic platinum. Specifically, the {002} type reflections of fcc Pt, at 0.197 nm, and {111} at 0.227 nm can be identified in the experimental DDP inset in the figure. The 55° angle that can be measured between these diffraction spots fits also very well with the expected value. This result confirms that the treatment with hydrogen at 423 K has transformed the platinum precursor into the metallic state.

In good agreement with previous observations on Rh/CeO_2 and Pt/CeO_2 catalysts,[7,13] the Pt particles adopt, in general, a shape close to that of a truncated cuboctahedron, exposing flat {111} and {002} facets. Only exceptionally, more complex morphologies could be

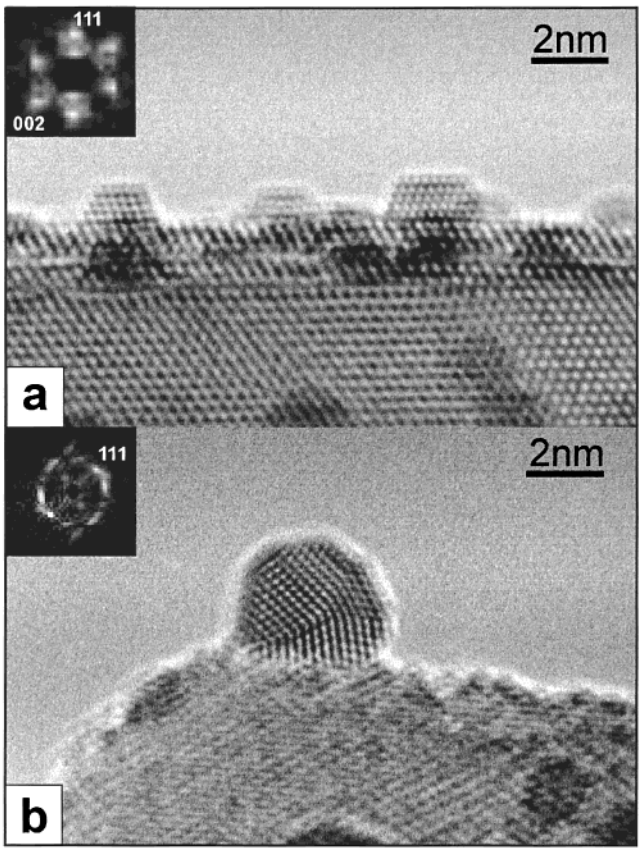

Figure 1. Representative HREM images of the 5% Pt/$CeTbO_x$ catalysts reduced at 423 K. DDPs insets in the figures were obtained from the particles sitting on the surface.

observed between the particles with large diameters, like that shown in Figure 1b. In the latter case, the ring of Pt-{111} reflections observed in the DDP suggests that the metal particle is constituted by a multiple twin.

In the catalyst reduced at 773 K, HREM images indicate that Pt is still present in the form of metallic particles. Thus, the 0.23-nm lattice spacing measured between the fringes imaged in the small particles observed in Figure 2, can be also reasonably assigned to that of {111} planes of Pt. In the support region on its hand, the 0.312-nm distance characteristic of the (111) planes in $CeTbO_x$ can be measured between lattice fringes. The assignment of these images to platinum particles on a mixed-oxide support has been confirmed using HREM image simulation. Figure 3a shows a simulated image that matches fairly well the contrasts observed in the experimental ones contained in Figure 2. As depicted in Figure 3b this simulation corresponds to a structural model containing a metallic platinum particle, with a (111)-truncated cuboctahedron shape and diameter close to 2.5 nm, sitting with the {111} face at the truncation on a {111} surface of the mixed oxide. The metal particle has been grown in a parallel orientation relationship with respect to the support[7] and next to a surface step of the oxide which runs parallel to one of its [110] edges. The whole metal−support system was tilted out of the [110] zone axis by a rotation of 15° around the $[1\bar{1}1]$ axis of platinum. It can be appreciated how the simulated image shows a fringe-like appearance both in the particle and support regions. The distance between the metal fringes is 0.23 nm, whereas that between the fringes of the support is close to 0.31 nm,

(27) Stadelmann, P. *Ultramicroscopy* **1987**, *21*, 131.

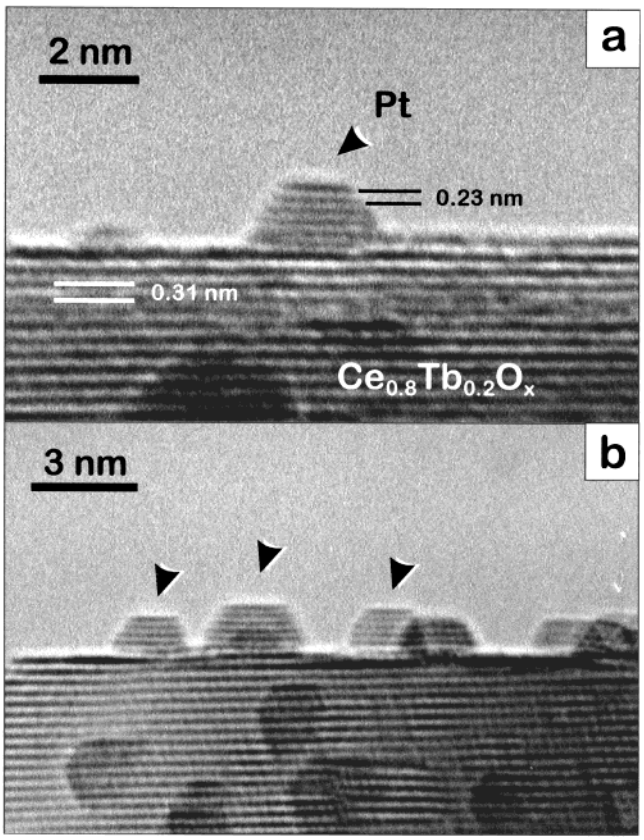

Figure 2. HREM images representative of the Pt/CeTbO$_x$ reduced at 773 K. The 0.23-nm lattice spacing marked in panel a corresponds to that of Pt {111} planes.

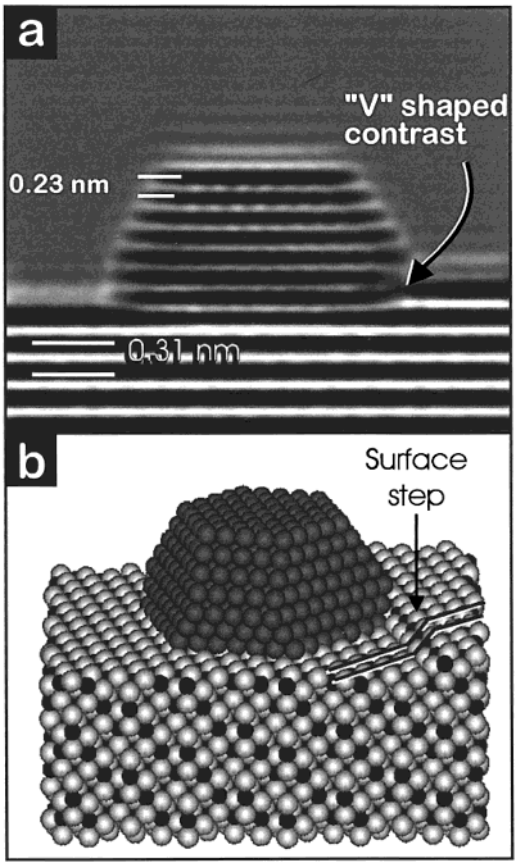

Figure 3. (a) Simulated image showing a Pt particle with {111} fringes parallel aligned with {111} fringes of the Ce−Tb mixed oxide. Simulation conditions: defocus = 50 nm; C_s = 0.7 mm, defocus spread = 10 nm, beam semiconvergence = 1.2 mrad. (b) Structural model employed to calculate the simulated image shown in part a. See the text for details about the model.

in good correspondence in both cases with the values estimated in the experimental images. The outline of the metal particle in the simulation resembles also quite well that observed in the experimental images.

The loss of bidimensional resolution in the experimental image in Figure 2 is due to crystal tilt. In effect, calculations reported in ref 14 indicate that tilts with very small amplitudes, about 7°, are large enough to degrade the resolution of the images of metal particles in the range size of those observed in Figures 1 and 2. Nevertheless tilts such as the one considered here, around an axis perpendicular to the metal−support interface, should not modify the lattice fringe spacing from the expected value.

Crystal tilt is also responsible for other fine details of the experimental images presented here for the catalyst reduced at 773 K and is worth comment. This is the case of the bending of the metal fringe contrasts observed at the bottom right corner of the contact region between the metal and the support, marked in Figure 3a. Intuitively, these contrasts could be interpreted as being due to atomic displacements or distortions at the boundaries between the metal particles and the support. A surface−interface reconstruction could be argued for as the driving force for these distortions. The calculation included in Figure 3a indicates nevertheless that this contrast effect could be simply the result of the combined influence on the image of crystal tilt and the presence of the support surface step in the vicinity of the metal particle. As a matter of fact, in the structural model employed for the calculation of Figure 3a no displacement of the atomic positions either in the metal particle or in the support, from those characteristic of the corresponding massive phases, have been considered. Despite that, the bent metal fringe contrasts are nicely reproduced in the calculated image. The occurrence of distortions does not seem, therefore, completely necessary to interpret these contrasts.

Another feature of interest in relation to the experimental HREM images of the catalysts reduced either at 623 K or at 773 K, is the alignment observed between the fringes of the metal particles and those of the support. This alignment is indicative of a growth of the metal particles under a parallel or twin topotactic relationship with the support, as previously described by us for Rh/CeO$_2$[7,13] and Pt/CeO$_2$[9,13] catalysts. The occurrence of these orientation effects reveals that at least a structural interaction is operating between the Pt metal particles and the CeTbO$_x$ support after reduction at low temperatures.

An interesting piece of information that can be also obtained from the analysis of these micrographs is that related to the size of the Pt particles in these catalysts. On the basis of HREM images, such as those presented in Figures 1 and 2, a direct estimate of the diameter of the metal particles can be obtained. Moreover, by measuring on tens of micrographs the diameter, as defined in ref 11, of several hundred metal crystallites, the size distribution of the metal phase for a given sample can be established. Figure 4a contains the

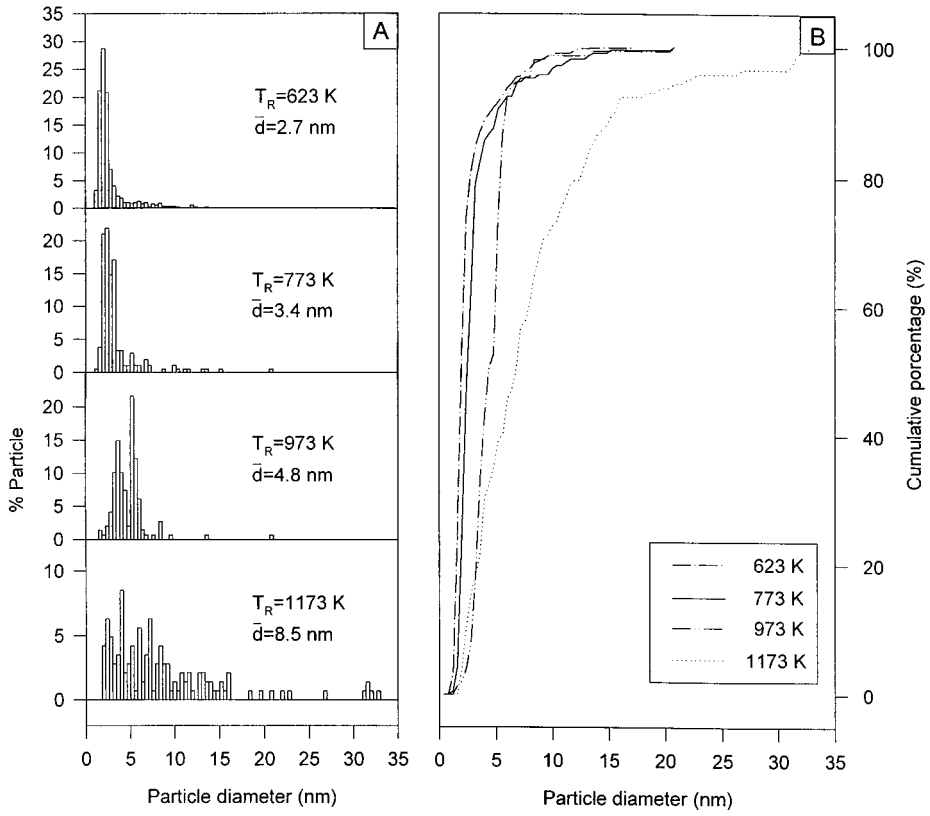

Figure 4. (a) Histograms corresponding to the particle size distribution established from the HREM images for the catalyst reduced at the different temperatures; Mean particle diameter values, $\bar{d}$, are indicated; and (b) cumulative curves estimated from the histograms.

histograms corresponding to the distributions of particle sizes of the Pt/$CeTbO_x$ catalyst after reduction at 623 and 773 K. As observed, the main core of both distributions is rather narrow, with 90% of the metal particles showing sizes below 5 nm (Figure 4b). It is also clearly observed in the cumulative distribution curves plotted in Figure 4b that the increase in reduction temperature from 623 K up to 773 K does not involve a significant change in the distribution of particle sizes, only a slight shift toward larger diameters being observed. From these histograms, a mean particle size of 2.7 nm can be computed for the catalyst reduced at 623 K and a slightly larger one, 3.4 nm, for that reduced at 773 K. Hence sintering does not seem to be very pronounced in the low reduction temperature range.

A final remarkable detail worth noting in relation to the images contained in Figures 1 and 2 is that the surfaces of the metal particles appear to be flat and clean.

3.2. Nanostructure of the 5% Pt/$CeTbO_x$ Catalyst after Reduction at High Temperatures (973−1173 K). The increase of the reduction temperature above 773 K gives rise to drastic changes in the nanostructure of the 5% Pt/$CeTbO_x$ catalyst. Thus, Figure 5 shows two representative views of the catalyst treated with flowing hydrogen at 973 K. In this case, although a metallic platinum phase is still present, the surfaces of the metallic particles appear now to be covered by a thin layer of a different material. Image processing on these overlayers indicates that they can be ascribed to support material. In effect, Figure 5a shows a platinum particle partially embraced by support layers. On the uppermost (111) plane of this particle a row of black dots, at a distance ~0.34 nm from each other, partially covering the surface, is evident. This distance is much larger than that corresponding to adjacent Pt atoms in the fcc structure and corresponds fairly well with the distance between neighboring lanthanide cations along the [1$\bar{1}$2] direction of the mixed oxide (0.33 nm). This result indicates that these black dot contrasts observed at the surface cannot be assigned to the structure of the metal particle but should instead be ascribed to a coverage by a {111} support layer.

Image calculation, Figure 6, further confirms this hypothesis. Thus, Figure 6a shows a simulated image that reproduces quite well the main contrast features observed in Figure 5a. According to the structural model employed for this calculation, Figure 6b, the black dot contrasts at 0.34 nm are due to a (111) $CeTbO_x$ cap covering the surface of the metal. As depicted in the cross section shown in Figure 6c, in this model the bottom half of the platinum particle is also surrounded by the $CeTbO_x$ crystallite. The contrast pattern observed in this region where the structure of the metal and the support overlap, looks essentially like that of the Ce/Tb mixed oxide, but other local contrast variations details that resemble those in the experimental image are also visible in the calculated image, as is the case of a lower local brightness. The boundaries of this lower brightness region allow one to roughly outline the shape of the particle. It is fairly clear in the experimental image shown in Figure 5a that the portion of support that surrounds the bottom part of the particle is well above the average height of the surface of the support crystallite which, in fact, is very flat. This suggests that the decoration process of the metal particles observed

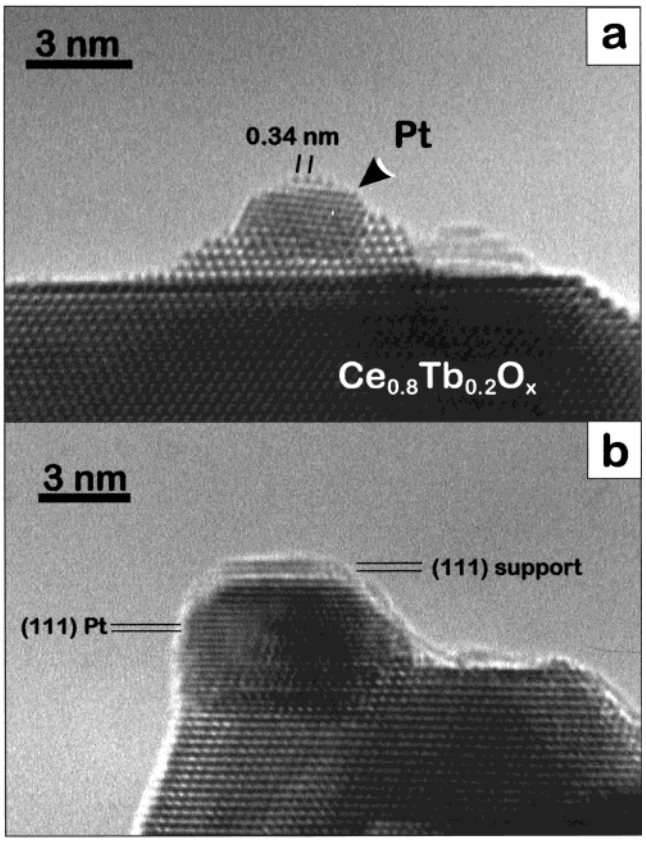

Figure 5. HREM images showing the main nanostructural features of the catalyst reduced at 973 K. Note in both cases, a and b, the presence of decorating layers on top of the platinum particles. The 0.34-nm distance marked in part a refers to the separation between black dots in the decorating monolayer.

after reduction at high temperature takes place by the support climbing over the metal particle surfaces rather than burial of the metal particle within the support. This result is in good agreement with the theoretical considerations reported by Sanchez et al.[28] for metals supported on oxides with the fluorite-type structure, as is the case of our $CeTbO_x$ oxide.

In the experimental image shown in Figure 5b evidence for the decoration effects is provided by the presence of two $CeTbO_x$ layers on top of the metal particle. As indicated in this figure, a 0.312 nm spacing, characteristic of the (111) planes of this mixed oxide, can be measured in this region of the micrograph with the aid of digital intensity profiles recorded along the direction normal to the decorating layers.

After reduction at 1173 K further transformations take place. Figure 7 shows two experimental images representative of treatment at this temperature. In this case the fringe patterns observed in the supported particles cannot be interpreted as being due to metallic platinum but, instead, in terms of an intermetallic compound with stoichiometry of the type $LnPt_5$ (Ln = Ce, Tb). Thus, the 0.46 nm × 0. 44 nm dot pattern observed in the particle contained in Figure 7a can be tentatively assigned to the [010] zone axis of a $LnPt_5$ phase, as indicated in the digital diffractogram inset in that figure. In a similar way, image 7b can be interpreted assuming a $LnPt_5$ intermetallic particle oriented along its [$\bar{1}$10] zone axis.

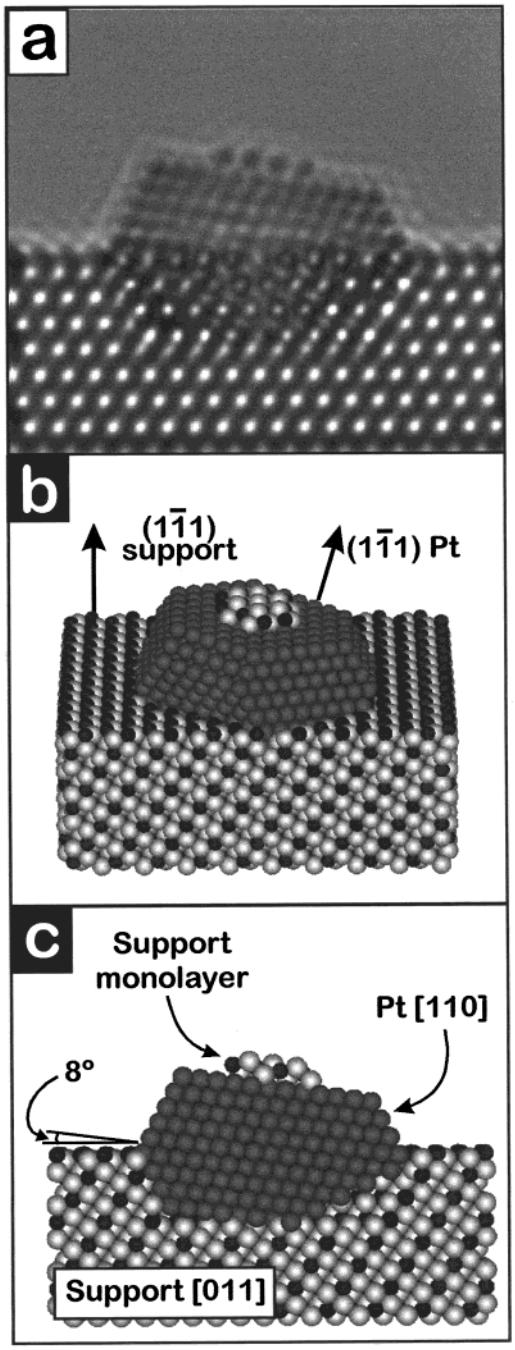

Figure 6. (a) Simulated image reproducing the main contrast features observed in Figure 4a. Note also in this simulation the presence of black dots separated by 0.34 nm on the surface of the platinum particle. (b) Structural model employed to calculate Figure 5a. Note the presence of a decorating cap on top of the (111) uppermost surface of the particle. (c) Cross-section of Figure 5b that shows more clearly how a particle partially embedded in the support has been considered for this calculation.

Among the different Ln−Pt intermetallic phases described in the literature,[29−33] hexagonal-$LnPt_5$ is the

(28) Sánchez, M. G.; Gazquez, J. L. *J. Catal.* **1987**, *104*, 120.

(29) Bronger, W. *J. Less-Common Met.* **1967**, *12*, 63.
(30) Le Roy, J.; Moreau, J. M.; Paccard, D. *Acta Crystallogr.* **1978**, *B34*, 9.
(31) Compton, V. B.; Matthias, B. T. *Acta Crystallogr.* **1959**, *12*, 651.

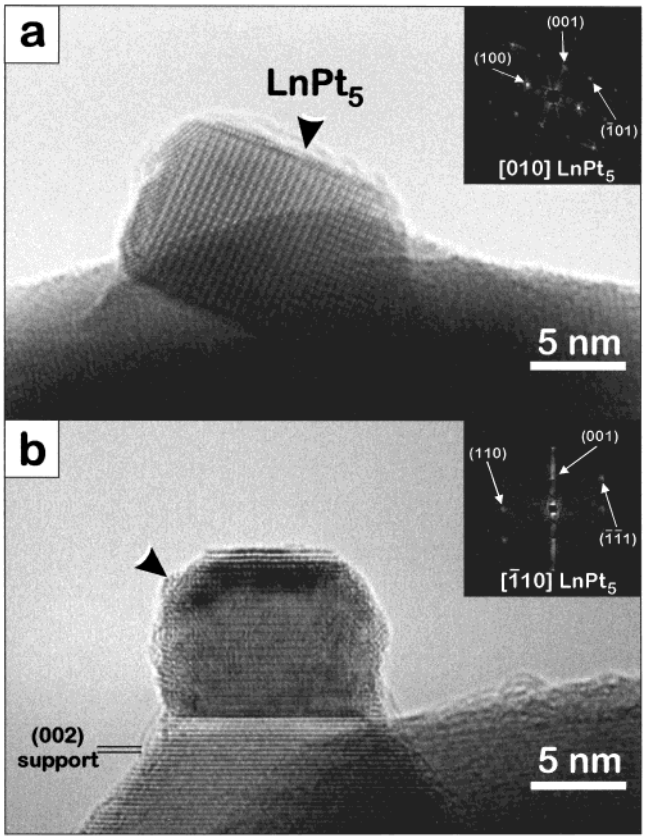

Figure 7. HREM images corresponding to the catalyst reduced at 1173 K. Insets correspond to digital diffractograms obtained on the supported particles that can be interpreted as due to the [010] zone axis (a) and the [$\bar{1}$10] zone axis (b) of an hexagonal $LnPt_5$ intermetallic compound.

only stoichiometry that could be identified in the whole set of experimental images recorded for the 5% Pt/$CeTbO_x$ catalyst treated at the highest reduction temperature. Such a result cannot be explained as being due to intrinsic detection problems, because each of the different intermetallic phases present at least one zone axis HREM image with characteristic geometric features that allow for their unequivocal identification.[9] Under these circumstances it seems likely that the above-mentioned intermetallic compound is the only one present in the catalyst after reduction at 1173 K. According to thermodynamic data available in the literature[34,35] about Pt−lanthanide intermetallics, $LnPt_5$ is the most stable for both Ce and Tb, $TbPt_5$ being, on the other hand, more stable than $CePt_5$.[35] These data point out that after 1 h of treatment in hydrogen at 1173 K the catalysts seem to reach equilibrium conditions and that the incorporation of the two lanthanide ions present in the support to the intermetallic compound is most likely.

The presence of a $LnPt_5$ intermetallic phase has been confirmed by electron diffraction in selected areas. In effect, in the diffraction patterns recorded on the catalyst reduced at 1173 K, Figure 8, different diffraction spots characteristic of this phase can be identified.

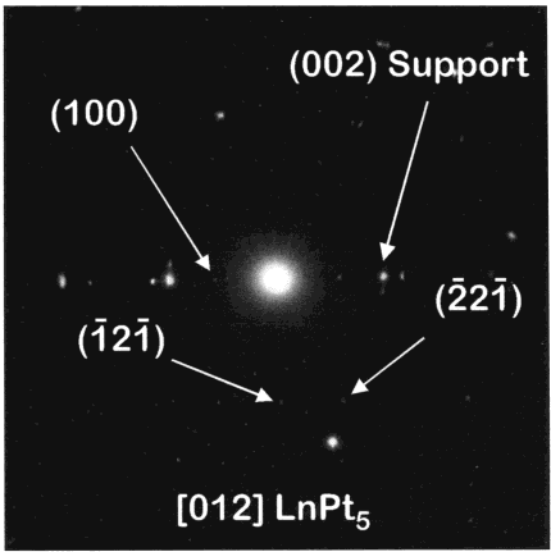

Figure 8. Selected area diffraction pattern recorded on the catalyst reduced at 1173 K. Note the presence of diffraction spots characteristic of $LnPt_5$ aligned with reflections coming from the mixed-oxide support.

Image simulation has allowed us, additionally, to determine the approximate shape of the intermetallic crystallites (Figure 9). According to images calculated for profile view (Figure 9b) and planar view images (Figure 9d), the preferential growth along the hexagonal *c* axis detected for most of the $LnPt_5$ particles, as shown in Figure 9a, can be interpreted assuming a beryl-type morphology. This type of morphology (Figure 10), involves a faceting of the intermetallic particle using {0001}, {10$\bar{1}$1} and {10$\bar{1}$0} planes of the hexagonal cell and corresponds to the equilibrium shape characteristic of crystals with space group *P*6/*mmm*,[36] as is the case of the $LnPt_5$ phases. This result would be in agreement with the idea that steady-state conditions are reached during the reduction treatment at 1173 K.

Another aspect worthy of comment in relation to the intermetallic is that specific orientation relationships have been found between the $LnPt_5$ alloy particles and the mixed oxide support. The images contained in Figure 9 are representative of one of these relationships. In this case the following relations can be established:

$$[010]_{LnPt5} \parallel [010]_{support} \quad (1) \qquad (1)$$

$$(001)_{LnPt5} \parallel (001)_{support} \quad (2) \qquad (2)$$

The parallel alignment of the (001) planes of $LnPt_5$ and the (002) planes of the support observed in Figure 7b or in the SAED pattern shown in Figure 8 is an example of a different orientation relationship between the support and the supported phase.

A further question that deserves some attention with regard to the influence of reductions at high temperature is their effect on the particle size distribution. As can be noted in Figure 4, increasing the reduction temperature above 773 K results in a significant broadening of the metal particle size distribution curves and, concomitantly, in a shift of the mean particle size to

(32) Le Roy, J.; Moreau, J. M.; Paccard, D. *Acta Crystallogr.* **1977**, *B33*, 2414.
(33) Dwight, A. E.; Conner, R. A.; Downey, J. W. *Acta Crystallogr.* **1985**, *18*, 835.
(34) Kleykamp, H. *J. Nucl. Mater.* **1993**, *193*, 201.
(35) Jacob, K. T.; Waseda, Y. *Bull. Mater. Sci.* **1990**, *13* (4), 235.
(36) Vainshtein, B. K. In *Modern Crystallography I*; Queisser, H.-J., Ed.; Springer-Verlag series in solid-state sciences; Springer-Verlag: Berlin, 1981; Vol 15, pp 204−206, ISBN, 3-540-10052-0.

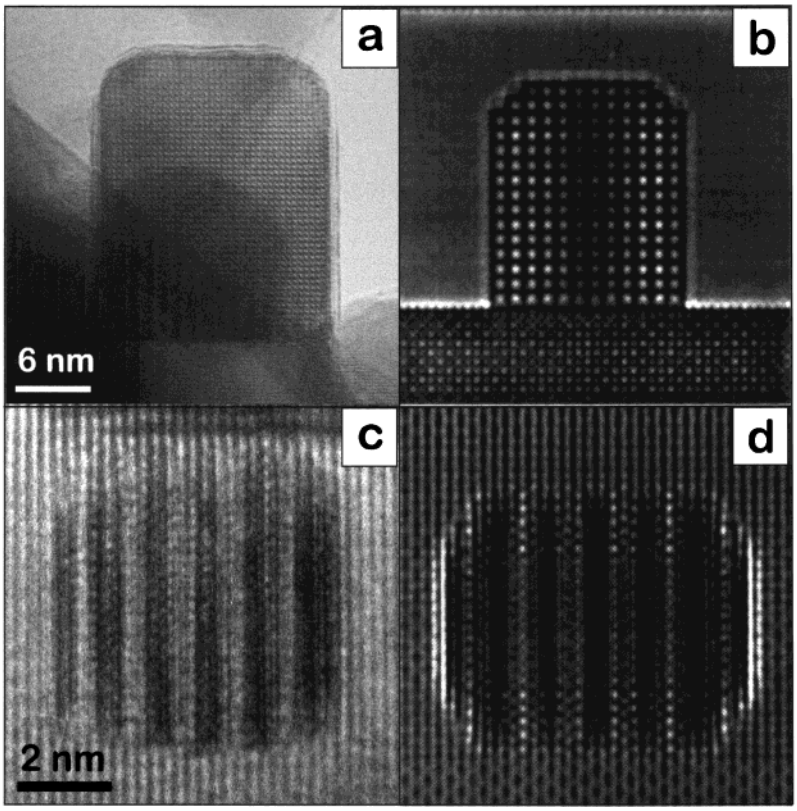

Figure 9. (a) Experimental HREM image, recorded in profile view conditions, obtained on the 5% Pt/CeTbO$_x$ catalyst reduced at 1173 K; (b) simulated image that matches the contrast and crystal shape observed in part a (in this case a beryl-type morphology has been assumed for the calculation); (c) experimental HREM, recorded in planar view conditions, corresponding to the catalyst reduced at 1173 K; and (d) simulated image reproducing the contrasts observed in part c.

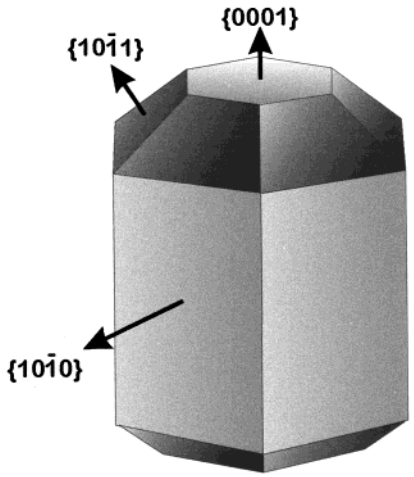

Figure 10. Sketch showing the typical faceting corresponding to the beryl-type morphology.

larger values. The metal sintering tendency is rather modest up to 973 K, becoming much stronger after reduction at 1173 K. In the last case the mean particle size is increased by an 80%. This effect is even more evident in the cumulative distribution curves plotted in Figure 4b, where a shift of the curve corresponding to the catalyst treated at 1173 K becomes obvious.

Taking into account the fact that according to the available crystallographic data,[29,37] the expansion of the unit cell associated with the transformation of Pt into $LnPt_5$ involves only a 13% increase in the lattice parameter, it is clear that the reduction treatment at 1173 K induces, in addition to the chemical changes, a significant growth of particles that contain platinum atoms.

3.3. Nanoanalysis (EELS) of the 5% Pt/CeTbO$_x$ Catalyst after Reduction at 1173 K. Alhough the drastic structural changes detected by HREM provide convincing evidence that the reduction treatment at 1173 K in pure hydrogen for 1 h leads to the alloying of Pt with the lanthanide elements present in the support to form a $LnPt_5$ intermetallic, a direct chemical analysis clue would be more conclusive at this respect. Such analysis could, additionally, provide information about the composition in each lanthanide element of this alloy, an aspect which, on the other hand, is not available through the analysis of the contrasts of the HREM images of the intermetallic particles. The subnanometric electron probe that can be generated in a FEG/STEM microscope, in combination with the analytical capabilities of EELS spectroscopy are especially well suited to obtain chemical information from nanometer-sized volumes.[38,39] Thus, to gain more precise information about the composition of the intermetallic phase formed after reduction at 1173 K, a set of EELS spectra was collected along a line scan of the electron beam, starting in a position at the bulk of a support crystallite, crossing the interface between the support and an intermetallic particle and ending in a bulk position of the supported

(37) Wernick, J. H.; Geller, S. *Acta Crystallogr.* **1959**, *12*, 662.

(38) Colliex, C. *J. Electron Microsc.* **1996**, *45*, 44.

(39) Bouchet, D.; Brun, N.; Imhoff, D.; Mory, C.; Stéphan, O.; Suenaga, K.; Tencé, M.; Williams, P.; Colliex, C. *Proc. Intern. Centennial Symp. On the Electron, Cambridge* **1997**, pp 253−264.

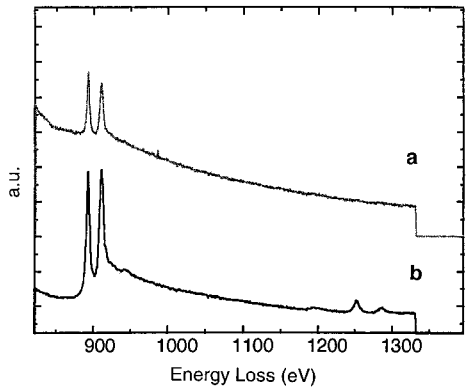

Figure 11. EELS spectra selected from a line-scan crossing a support/particle interface in the catalysts reduced at 1173 K: (a) spectrum from a position within the supported particle; and (b) spectrum from the $CeTbO_x$ crystallite underlying the particle.

particle. The range of energy losses corresponding to the M4 and M5 edges of Ce and Tb was recorded at 1-nm steps along this line. The analysis of the modifications taking place in the fine structure of this set of ELNES line spectra allows us to study the changes in the chemical and electronic properties of the material through the interface.[40] Figure 11 shows the ELNES spectra corresponding to two points in the line scan located at positions far from the interface. The spectrum in Figure 11a was recorded from a position within the supported particle, whereas that in Figure 11b corresponds to a point at the support. In the spectrum recorded on the support the peaks corresponding to the M4 and M5 white lines of Ce, about 900 eV, and those of Tb at 1250 eV, are clearly observed.[41] A weak and wide signal, around 1200 eV, characteristic of the Ce M3 edge[41] is also present. In the spectrum recorded on the particle (Figure 11a), the peaks of the Ce-M4 and -M5 edges are also present, whereas no Tb signal is visible in principle. By taking into account that the diameter of the electron probe generated in the VG HB501 used in this study is only about 1 nm and that the spectrum was obtained from a particle located on the surface in profile projection, in a position inside the particle a few nanometers apart from the interface, it can be ruled out that this Ce signal comes from the support. Hence, this result proves directly the formation of the intermetallic and suggests, on the other hand, a preferential incorporation of cerium into the intermetallic.

Figure 12 shows spectra recorded in the energy- loss region corresponding to the Ce M4 and M5 edges but with a higher energy resolution (0.6−0.8 eV). The spectrum in Figure 12a was obtained on the support and that in Figure 12b on one particle. A careful comparison of these figures reveals that the peaks in the spectrum of the particle are shifted by 1.8 eV toward lower energies with respect to those observed in the spectrum of the support. This shift is related to a difference in the oxidation state of cerium between the support and the particle. The positions, in the energy

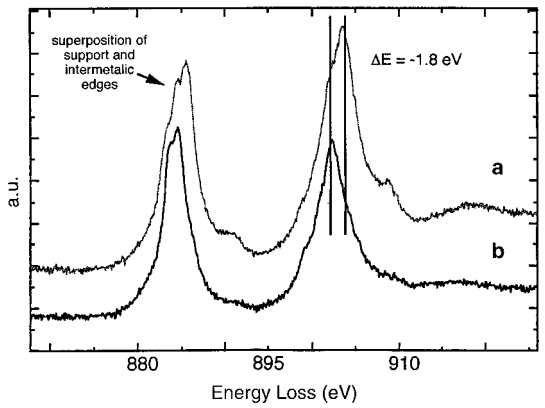

Figure 12. High-resolution EELS spectra, in the energy-loss region characteristic of the Ce M4,5 edges, recorded on the catalyst reduced at 1173 K.

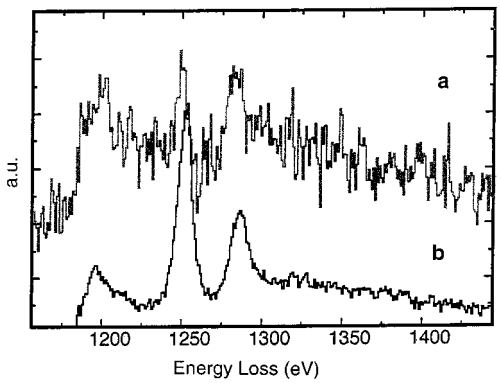

Figure 13. Enlargement of the spectra in Figure 11 in the energy-loss region characteristic of Tb edges.

loss scale, of the peaks in Figure 12a correspond to those of Ce(4+) in CeO_2[42] whereas those observed in Figure 12b are very close to those of Ce in compounds such as $CePd_3$, $CeAl_2$, or γ-Ce[42] and, therefore in, at least formally, a more reduced oxidation state. Other fine details such as the change in the relative intensities of the M4 and M5 peaks, the disappearance of the small shoulders observed at the right of each peak in the spectrum of Figure 12a, and the appearance of complexities at the left-hand side of the peaks in the spectrum of Figure 12b are also in good agreement with the idea of a decrease in the oxidation state of cerium within the particle. In other words the analysis of the fine structure of the ELNES spectra is also consistent with the formation of an intermetallic compound between Pt and, at least, Ce.

Likewise, a more detailed analysis of the spectra in Figure 11 in the energy range 1100−1400 eV, which are shown enlarged in Figure 13, allows one to refine the conclusions about the Tb content of the intermetallic. In effect, a comparison of the signal obtained in the intermetallic (Figure 13a) with that recorded in the support (Figure 13b) suggests the presence of some traces of Tb in the intermetallic. Given that the Tb signal is too weak, a precise quantitative estimate of the Ce/Tb ratio in the intermetallic cannot be obtained. The intrinsic problems associated to the use of white lines for quantitative analysis, the overlap of the Ce M2

(40) Colliex, C.; Tencé, M.; Lefévre, E.; Mory, C.; Gu, H.; Bouchet, D.; Jeanguillaume, C. *Mikrochim. Acta* **1994**, *114/115*, 71.

(41) Ahn, C. C.; Krivanek, O. L.; Burgner, R. P.; Disko, M. M.; Swann, P. R. In *EELS Atlas*; Gatan Inc.: Warrendale, PA; and ASU HREM Facility: Tempe, AZ, 1983.

(42) Kaindl, G.; Kalkowski, G.; Brewer, W. D.; Perscheid, B.; Holtzberg, F. *J. Appl. Phys.* **1984**, *55* (6), 1910.

and Tb M4 edges and the differential influence on the intensity of the white lines due to the change in the oxidation state of Ce and Tb when forming the intermetallic preclude also any possibility of performing a quantitative treatment of the spectra included in Figure 13 and, therefore, obtaining a precise value of the Ce/Tb ratio in the intermetallic. Nevertheless it can be stated qualitatively from these spectra that this ratio is much higher in the intermetallic than in the support, and that cerium is the lanthanide which incorporates predominantly to the intermetallic particles, which should have a composition very close to $CePt_5$.

The spectrum shown in Figure 11b, in which the intensities of the Tb signals are not as weak as in the case of those recorded in the spectrum of the intermetallic, can be analyzed in order to obtain an estimation of the Ce/Tb ratio in the support. The procedure for extracting this information is complex but essentially involves the following consecutive steps:[43] (1) correction of multiple scattering effects, whose intensity is thickness dependent, by deconvolution of the core loss signals with the zero-loss signal obtained at the same point in the sample where the ratio is being analyzed; (2) removal of the background of the signals by extrapolation of the exponential curve that allows the best fit with the preedge data; and (3) fitting of the deconvoluted, background-corrected spectrum with calculated cross sections and simulated Lorentzian-type white lines. The Hartree−Slater method was used to simulate the shape of all cross sections. A specific program developed by the Orsay group was used to perform the fitting step. The Ce/Tb ratios estimated from a set of experimental spectra recorded in a number of positions within different support particles were, in all cases, close to each other, with a maximum deviation of about 7%. This result indicates that segregation does not seem to take place after the reduction treatment at 1173 K.

Conclusions

The combined application of HREM, image simulation/processing, and EELS spectroscopy has allowed us to investigate the details of the structural and chemical changes taking place, at nanometer scale, in a 5% Pt/$Ce_{0.8}Tb_{0.2}O_{2-x}$ catalyst reduced in flowing hydrogen at temperatures ranging from 423 K up to 1173 K. Up to 773 K, the reduction treatment gives rise to a system containing platinum particles with clean surfaces. The metal particles are grown onto the support under certain, well-defined, orientation relationships. This latter fact provides evidence for the existence of, at least, a structural interaction between the support and the supported metal particles. For the catalyst reduced at 973 K, the nature of the metal−support interaction effect changes significantly. As revealed by our HREM images, platinum microcrystals appear decorated by a thin support layer. At the highest reduction temperature considered in this study, the presence of the platinum particles favors a deep reduction of the rare earth oxide by stabilizing the formal zerovalent rare earth atoms in the form of an intermetallic compound with a hexagonal-$LnPt_5$ structure. HREM image simulation has explained the preferential growth observed for the alloy particles as being due to a beryl-type morphology.

EELS spectroscopy has added a chemical dimension to the analysis of the evolution undergone by our catalysts as a consequence of the thermochemical treatments here considered. The application of this technique has allowed us to retrieve valuable data about the composition of both the supported particles and the support at a very fine spatial scale. These results confirm and refine the conclusions obtained from the structural study carried out using HREM. Specifically, the analysis of the fine structure of ELNES spectra recorded in the catalyst reduced at 1183 K has undoubtedly confirmed the incorporation of both lanthanide elements, present in the support crystallites, into the supported particles observed after this treatment. The detailed comparison of the relative intensities of the white lines of Ce and Tb in these ELNES spectra, suggests also a significant increase of the Ce/Tb ratio in the intermetallic particles with respect to that characteristic of the support crystals. Hence, contrary to the expectations based on thermodynamic data, preferential incorporation of cerium in the intermetallic phase seems to take place during the alloying process. Additionally, EELS spectra have allowed us to confirm that Ce and Tb are homogeneously distributed, on a nanometer scale, in the mixed oxide crystals. Moreover, no segregation phenomena take place even after a treatment as severe as a reduction in pure H_2 at 1173 K during 1 h.

In summary, the whole set of HREM images and EELS spectra obtained in this study allows us to propose an approximate picture of the evolution of metal support interaction effects in a new family of catalysts, Pt/$CeTbO_x$, with potential applications as a TWC component.

Acknowledgment. This work has received financial support from DGICYT (PB95-1257) and CICYT (MAT96-0931). The experimental images were recorded at the EM Facilities of the SCCYT of the Universidad de Cádiz. Support of J. A. Pérez-Omil at the University of Orsay was obtained from a Marie Curie fellowship.

CM991093Q

(43) Manoubi, T.; Colliex, C.; Rez, P. *J. Electron Spectrosc. Relat. Phenom.* **1990**, *50*, 1.